8-27-2024

Experimental Realization of Supergrowing Fields

Sethuraj K. R.

Tathagata Karmakar

S. A. Wadood

Andrew N. Jordan

A. Nick Vamivakas

Experimental Realization of Supergrowing Fields

Letter

Experimental realization of supergrowing fields

Sethuraj K. R.,[1,2,*] Tathagata Karmakar,[2,3,4,†] S. A. Wadood,[1,2,5] Andrew N. Jordan,[2,3,4] and A. Nick Vamivakas[1,2,3,6,‡]

[1]*The Institute of Optics, University of Rochester, Rochester, New York 14627, USA*

[2]*Center for Coherence and Quantum Optics, University of Rochester, Rochester, New York 14627, USA*

[3]*Department of Physics and Astronomy, University of Rochester, Rochester, New York 14627, USA*

[4]*Institute for Quantum Studies, Chapman University, Orange, California 92866, USA*

[5]*Currently with Department of Electrical Engineering, Princeton University, New Jersey, 08544, USA*

[6]*Materials Science, University of Rochester, Rochester, New York 14627, USA*

(Received 15 September 2023; revised 5 March 2024; accepted 17 July 2024; published 27 August 2024)

Supergrowth refers to the local amplitude growth rate of a signal being faster than its fastest Fourier mode. In contrast, superoscillation pertains to the variation of the phase. Compared to the latter, supergrowth can have exponentially higher intensities and promises improvement over superoscillation-based superresolution imaging. Here, we demonstrate the experimental synthesis of controlled supergrowing fields with a maximum growth rate of ∼19.07 times the system bandlimit. Our work is an essential step toward realizing supergrowth-based far-field superresolution imaging.

DOI: 10.1103/PhysRevResearch.6.L032043

Introduction. Superresolution in optical imaging refers to approaches that can boost spatial resolution beyond the diffraction limit of light. The diffraction limit defines the smallest feature size that can be resolved in a standard optical imaging system and is determined by the lights wavelength and the optical system's numerical aperture (NA) [1]. One way to resolve subwavelength features in far-field imaging is by using superoscillatory optical spots, a phenomenon where complex fields can locally oscillate at a rate greater than their cut-off spatial frequency [2–5]. Nonetheless, superoscillations have the inherent disadvantage of very small intensity combined with substantial side lobes, leading to poor imaging quality. Both numerical optimization schemes [6] and sophisticated optical setups [7–9] have been investigated for the mitigation of sidelobe intensity. However, supergrowth [10], a recently introduced physical concept, offers a promising route to solve this issue.

In supergrowing fields, the local amplitude growth rate of a complex field is higher than the highest spatial frequency in its Fourier spectrum, thereby also providing access to subwavelength features [11]. This concept has parallels to near-field microscopy with evanescent waves [12,13]. Supergrowing optical field spots can contain exponentially more intensity compared to superoscillating regions and have been shown theoretically to be able to image subwavelength objects [14]. Moreover, theoretical frameworks for systemic generation of both supergrowing/superoscillating fields have been studied [15]. Currently, supergrowth exists as a purely theoretical construct and has not been realized experimentally.

In this work, we achieve a critical step toward the goal of superresolution using supergrowth, i.e., the synthesis and characterization of supergrowing fields in the laboratory. To accomplish this objective, we elucidate the concept of supergrowth in a diffraction-limited system and identify the critical constraints that can limit supergrowth in an experiment. We also furnish comprehensive methods and tools to quantify supergrowth in any experimental setup effectively. The experimental demonstration lays the foundation for generating supergrowing fields that can be utilized for superresolution imaging.

Supergrowing strength. The local growth rate $\kappa(x)$ and local wave number $k(x)$ of a bandlimited normalized complex field $f(x)$ are defined as $\kappa(x) = \Re\, \partial_x \log[f(x)]$ and $k(x) = \Im\, \partial_x \log[f(x)]$ [11]. Therefore, $k(x)$ denotes the local rate of change of the phase of $f(x)$, while $\kappa(x)$ refers to the local amplitude growth rate. The field has supergrowth (superoscillation) at $x = x_0$ when $|\kappa(x_0)| \geqslant k^f_{\max}(|k(x_0)| \geqslant k^f_{\max})$, where $k^f_{\max}$ denotes the highest wavenumber of the field. To characterize the amount of supergrowth, we define the supergrowing strength $\Gamma(x) = |\frac{\kappa(x)}{k^f_{\max}}|$; $f(x)$ is supergrowing at $x = x_0$ when $\Gamma(x_0) \geqslant 1$.

The intensity $I(x) = |f(x)|^2$ has a bandlimit of $2k^f_{\max}$ and the local intensity growth rate $\kappa_I(x) = 2\kappa(x)$. The supergrowing strength $\Gamma(x)$ can be obtained from the intensity as

$$\Gamma(x) = \left|\frac{\kappa_I(x)}{2k^f_{\max}}\right|. \tag{1}$$

Equation (1) has significant implications in the experiment, as we need only the transverse intensity information, which

*Contact author: skarimpa@ur.rochester.edu

†Contact author: tkarmaka@ur.rochester.edu

‡Contact author: nick.vamivakas@rochester.edu

can be obtained using a CCD camera. For field-based experimental characterization of growth rate, one needs full-field reconstruction involving more complicated interferometry.

Supergrowth in a diffraction-limited optical system. The wavelength of illumination λ and an optical system's NA define its diffraction-limited response and maximum spatial frequency ($k^s_{\max} \approx \frac{2\pi}{\lambda}\text{NA}$) that can pass through the system [1]. The bandlimit of the optical system might be different from the field bandlimit $k^f_{\max}$, although the latter must be upper bounded by the former (i.e., $k^f_{\max} \leqslant k^s_{\max}$). We note that superresolution imaging using superoscillation/supergrowth is only possible when the local wavenumber/growth rate of the illumination field is higher than the bandlimit of the system $k^s_{\max}$. For $k^f_{\max} \leqslant |k|, |\kappa| < k^s_{\max}$, superresolution cannot be achieved.

For supergrowth in experiments, the appropriate definition is $|\kappa(x)| \geqslant k^s_{\max}$, so that the benefit of supergrowth can outperform the diffraction-limited performance of an optical system. The supergrowing strength of an optical field in an experiment is

$$\Gamma_s(x) = \left|\frac{\kappa_I(x)}{2k^s_{\max}}\right|, \tag{2}$$

where the subscript s in Γ_s indicates that it is defined with respect to the bandlimit of the system. According to this definition, the field $f(x)$ is supergrowing when $\Gamma_s \geqslant 1$. The optical fields realized in our experiment are supergrowing with respect to both definitions. For convenience, we define the bandlimit ratio $b = (k^f_{\max})/(k^s_{\max})$, such that $\Gamma_s = b\,\Gamma$.

Figure 1 provides an example of an optical field with different $\Gamma_s(x)$ and $\Gamma(x)$. One can observe that at some points $x = x_0$, the optical field is supergrowing in a mathematical sense ($\Gamma \geqslant 1$), but not supergrowing ($\Gamma_s < 1$) based on the definition we use. From here onwards, we stick to the definition of supergrowth strength as Γ_s.

Experiment. The schematic of the optical setup used to generate supergrowing optical fields is shown in Fig. 2: A computer-generated phase-only pixelated hologram (CGPPH) created using a liquid-crystal-based SLM (Hamamatsu LCOS). An intensity-stabilized 795 nm linearly polarized collimated laser beam (Toptica TA 100) is expanded using lenses L_1 and L_2 to ensure it overfills the active area of the SLM. As a result, the CGPPH sees less spatial variation in the intensity of the illuminating laser and a nearly uniform phase. To stabilize the laser intensity, an acousto-optic modulator with a PID controller is used, and polarization optics and attenuators are used to control the polarization and intensity of the laser beam (not shown in the schematic). The diffraction from the CGPPH is Fourier processed using a classical $4f$ processor consisting of lenses L_3 and L_4, and a precision pinhole P (Thorlabs P1000K). The intensity distribution of the complex field at the image plane (Z_I) is measured using a CCD camera. We have ensured the output intensity lies within the linear response of the detector.

Phase and amplitude of the optical field at coordinates (u, v) in the transverse plane Z_F determine the phase and amplitude of image plane (Z_I) Fourier components at $f_x = \frac{u}{\lambda f}$ and $f_y = \frac{v}{\lambda f}$ [1]. The maximum spatial frequency at the image plane is limited by the diameter d of the precision pinhole at Z_F, and the system bandlimit is $k^s_{\max} = \frac{\pi d}{\lambda f}$.

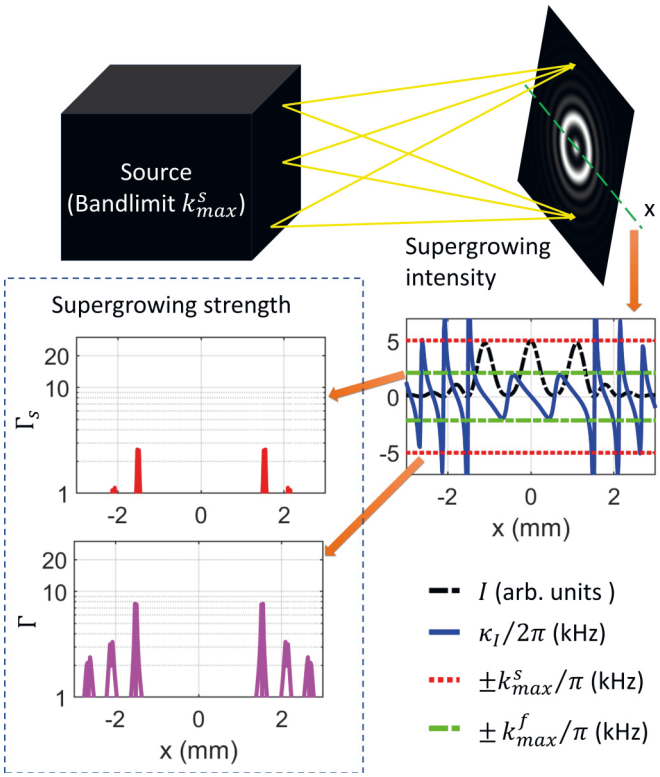

FIG. 1. Conceptual illustration of the dependence of supergrowth on field and system bandlimits. The optical source (shown as a black box) of bandlimit $k^s_{\max}$ synthesizes a supergrowing complex field (of bandlimit $k^f_{\max}$) at the image plane. Horizontal line cut of intensity $I(x)$, and supergrowing strength parameters $\Gamma(x)$ from Eq. (1) and $\Gamma_s(x)$ from Eq. (2) are plotted for a sample function. Since $k^s_{\max} \geqslant k^f_{\max}$ in any diffraction-limited optical system, the condition $\Gamma_s \geqslant 1$ is more restrictive in comparison to $\Gamma \geqslant 1$. This fact is manifested in the plot since a smaller region is identified by $\Gamma_s \geqslant 1$.

Generation of supergrowing functions. The CGPPH used in the experiment for generating a supergrowing function uses encoding techniques described in [16]. The function to be prepared in the experiment must satisfy two criteria: (i) bandlimit—$k^f_{\max} < k^s_{\max}$; and (ii) spatial limit—the distribution of the supergrowing field at the image plane Z_I must remain within the image of the SLM active area at Z_I. It is a challenge to satisfy both of these criteria as limitations imposed in the spatial domain demand a scaling up in the frequency domain. Larger values of $k^f_{\max}$ are necessary to ensure maximum supergrowth $\Gamma_s \geqslant 1$ within the spatial limit. Theoretically, $k^f_{\max} = k^s_{\max}$ is possible, but due to experimental imperfection and uncertainties, one cannot achieve this upper limit for a field in experiments.

We use two different ways of constructing supergrowing functions: (i) heuristic analytical method, and (ii) numerical optimization method. In the first approach, we use an analytical function $f(x, y) = f_1(x, y)f_2(x, y)$. The function $f_1(x, y) = \exp(\frac{-x^2-y^2}{2c^2})$ utilizes the constant c to confine the spatial extent of $f(x, y)$, and $f_2(x, y) = \cos(k_{f_2}[\rho - \rho_0]) + ia\sin(k_{f_2}[\rho - \rho_0])$ is normalized to unit maximum amplitude,

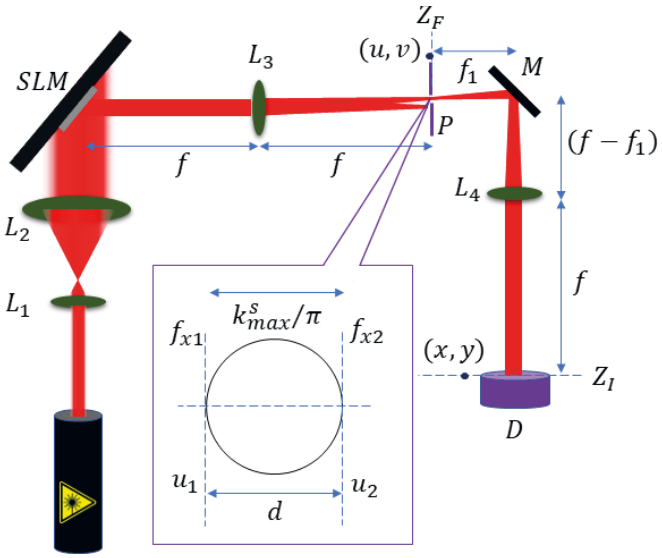

FIG. 2. Optical setup schematic. Notations: L, lens; SLM, Spatial light modulator; f, focal length of lens; Z_F; transverse back focal plane of L_3; P, precision pinhole; M, mirror; D, CCD camera; Z_I, image plane; (u, v), Cartesian coordinates representing any point on the plane Z_F; (x, y), Cartesian coordinates representing any point on the plane Z_I; d, diameter of P; and f_{x1} and f_{x2}, are horizontal (x) Fourier coordinate of Z_I. The inset shows an expanded view of the transverse cross section of P.

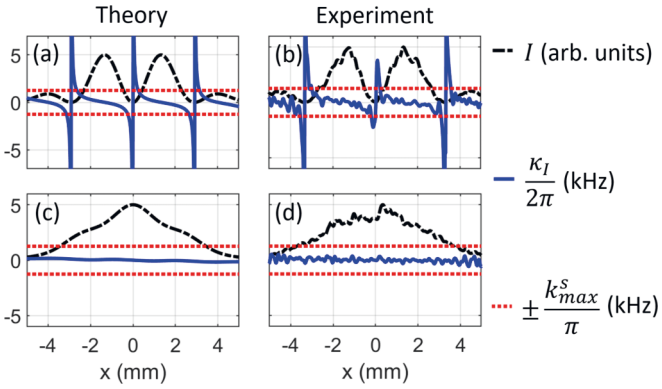

FIG. 3. Theory [(a) and (c)] and experimental [(b) and (d)] construction of optical fields with and without supergrowth. The upper row [(a) and (b)] depicts a field exhibiting supergrowth. The lower row [(c) and (d)] illustrates a field without supergrowth. Each plot [(a)–(c)] shows x-line cut of I and κ_I, along with $2k^s_{\max}$, identifying the supergrowing regions [Eq. (2)]. These plots substantiate our capability to engineer and manipulate supergrowth in optical fields experimentally.

where a is another constant. Here, ρ is defined as $\rho^2 = x^2 + y^2$ to ensure circular symmetry, and as $\rho = x$ to facilitate supergrowth horizontally. The shift ρ_0 can ensure the maximum or minimum of $|f_2(x, y)|$ to be at $\rho = 0$. The inspiration behind $f_2(x, y)$ comes from the $1D$ function $f(x) = (\cos x + ia \sin x)^N$, whose supergrowing properties have been studied in [11,14]. We choose $k_{f_2} \gg k_{f_1}$, where k_{f_1} is four times the full width half maximum of the Fourier transform of $f_1(x, y)$. The bandlimit criterion is satisfied as $k_{f_2} + k_{f_1} = bk^s_{\max}$, where $0.75 \leqslant b \leqslant 0.95$. Then, $f(x, y)$ supergrows locally when $a \gg 1$.

For experiments, we need optical fields with high supergrowing area (defined later) and high fractional intensity within the supergrowing regions. The analytical functions, characterized by only three parameters, have a limited ability to generate such fields. The numerical optimization method helps us overcome this obstacle. To find the appropriate fields that supergrow within the frequency and space limit on the image plane Z_I, we perform simulations using the Zernike polynomial-Bessel function basis for circular symmetric functions, and simultaneously adopt the Helmholtz equation-based definition of local wavenumber/growth rate (Appendices E and F of Ref. [15]). A multiobjective cost optimization is performed to ensure (i) optimum extent of supergrowing region within the image plane, (ii) optimization of the ratio of maximum intensity within the supergrowing region and the maximum intensity in the image plane. The second condition ensures the effect of enhanced sidelobes, a limitation observed in superoscillation-based superresolution imaging, is curtailed [6].

Supergrowing area Υ_s of measured image. Supergrowing area denotes the fraction of the area of a complex field that is supergrowing at the image plane. Υ_s is another tool for quantifying the quality of the supergrowing field—a higher value of Υ_s is better. But this definition of Υ_s is inadequate for images obtained from the experiment due to noise. Let $f(x, y)$ be the complex field at the image plane (Fig. 2). In the experiment, the CCD measures the spatially discretized and noisy version of intensity $I(x, y) = |f(x, y)|^2$ as $I_0(m, n)$, where m, n are matrix indices of the matrix representing CCD pixels. We have ensured the maximum spatial frequency of the field is much smaller than the frequency of the CCD pixels so that the Nyquist criterion is not violated. One can express $I_0(m, n) = \eta_d(m, n)I(m, n) + I_\xi(m, n)$, where $\eta_d(m, n)$ is the detection efficiency of the pixel (m, n), $I_\xi(m, n)$ is the noise, and $I(m, m)$ is discretized $I(x, y)$. The intensity quantization at each pixel is ignored in this representation.

Let the maximum value of the noise $I_\xi(m, n)$ be $I_{\xi 0}$. One cannot consider pixels with intensities $I_0(m, n) \leqslant I_{\xi 0}$. The supergrowing area of measured images can be defined as

$$\Upsilon_s = \frac{\zeta_s}{\zeta}, \tag{3}$$

where ζ is the total number of pixels with $I_0(m, n) \geqslant I_{\xi 0}$, and ζ_s is the total number of pixels with $\Gamma_s(m, n) \geqslant 1$ and $I_0(m, n) \geqslant I_{\xi 0}$.

Results. We have prepared multiple bandlimited complex functions with finite spatial extent using analytical expression and numerical optimization methods. The fields realized in the experiment have a diverse range of supergrowing strength Γ_s and area Υ_s.

Figure 3 demonstrates the ability to control supergrowth in the experiment. It shows representative fields with and without supergrowth, both in theory and in experiment. Both fields are synthesized using analytical functions, with $c = 3$ mm, $\rho = x$, $\rho_0 = 0$, and $b = 0.75$. For supergrowing fields, $a = 10^9$; for

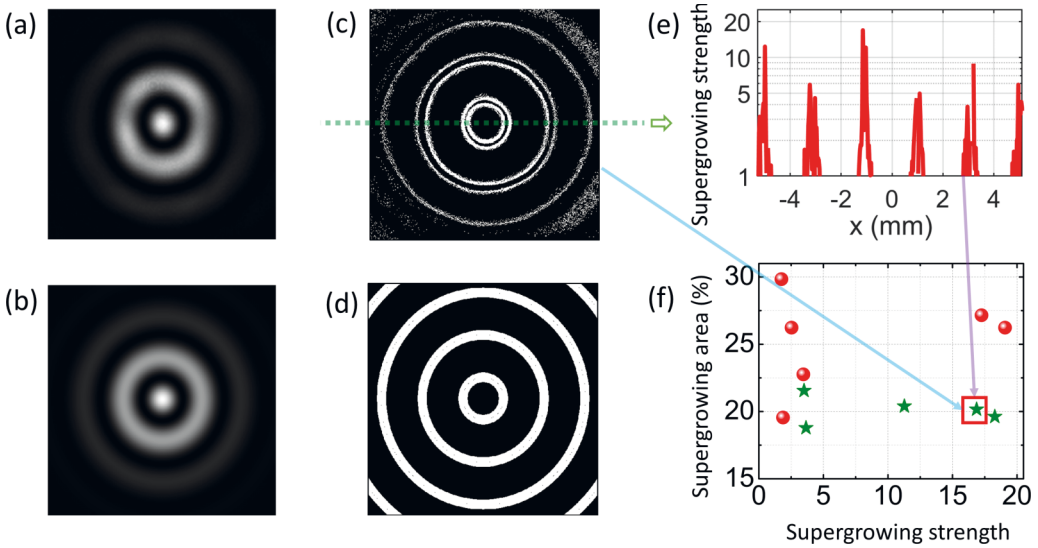

FIG. 4. Intensity of a synthesized field at the image plane z_I (Fig. 2), measured using the CCD, is shown in (a) and the corresponding analytical function is shown in (b). Panels (c) and (d) identify the supergrowing regions of measured and theoretical fields, respectively, in white. Supergrowing strength Γ_s of supergrowing regions identified in (c) along a horizontal line cut (highlighted using a semitransparent dashed green line) is shown in (e). We have averaged four adjacent rows of pixels to get this line cut to reduce the effect of noise. Panel (f) shows the quality of supergrowth of multiple fields, synthesized in the experiment, represented here by plotting supergrowing area Υ_s and maximum supergrowing strength Γ_s along the x linecut of each field. Here, red (green) spheres (stars) represent the function obtained using the numerical optimization method (heuristic analytical method). The field shown in (a)–(e) is highlighted using a red square in (f). We observe that numerical optimization enhances the range of the supergrowing area, achieving experimental Υ_s values ranging from 19.5% to 29.8%.

nonsupergrowing fields, $a = 0.9$. Row (1) of the figure shows a supergrowing field with a maximum of $\Gamma_s \approx 37.22$ ($\approx$18.28, in the experiment). The field shown in row (2), however, is not supergrowing [$\Gamma_s(x) < 1, \forall\, x$], both in theory and experiment.

A transverse distribution of intensity and corresponding supergrowing regions at the image plane Z_I [Fig. 2] of a representative complex field (both in theory and experiment) are demonstrated in Figs. 4(a)–4(d). The supergrowing area of this field is $\Upsilon_s \approx 23.6\%$ ($\approx$20.16%, in the experiment). The experiment exhibits lower Υ_s and double-ring patterns [Fig. 4(c)] because pixels with intensities less than the cutoff $I_{\xi 0}$ [Eq. (3)] are ignored. Note, for such $2D$ images of intensity $I(x, y)$, we calculate the local intensity growth rate as $\kappa_I(x, y) = |\nabla \log [I(x, y)]|$. By definition, supergrowth is more sensitive to fluctuations at low intensities. In the experiment, noise/distortions present at intensities comparable to the noise floor can lead to identifying more supergrowing regions than the analytical field. The definition of Υ_s [Eq. (3)] reduces this effect by neglecting low-intensity pixels.

Measured values of the supergrowing area Υ_s and the maximum values of supergrowing strength Γ_s for multiple supergrowing fields synthesized in the experiment are shown in Fig. 4(f). One can observe that the functions obtained from the numerical optimization method, in general, can attain larger values of Υ_s. See the Supplemental Material [17] for further information on the numerical optimization method, comparison with fields generated by the analytical method, and additional details about the optical fields used in the experiment. This is consistent with the multiobjective optimization conditions described previously. We have achieved a significantly larger supergrowing area (up to $\Upsilon_s \approx 29.84\%$) as well as a maximum local growth rate reaching up to $\approx$19.07 times the bandlimit of the system. A supergrowing strength of $\sim$19 is highly desirable since optical spots with high local growth rates help us image subwavelength objects.

Discussion. Supergrowth is a new physical phenomenon, and we have achieved the experimental demonstration of supergrowth in a controlled laboratory setup. We also prescribe comprehensive methods and parameters to measure and characterize the supergrowth in an experiment. In this context, we have clarified the distinction between the supergrowth of an optical field and the concept of supergrowth in a diffraction-limited optical system. While the latter provides a stronger constraint on the condition of supergrowth, we are still able to achieve local growth rates more than an order of magnitude higher in our setup compared to the system bandlimit. Additionally, our setup shows excellent control over supergrowth since we realize optical fields with a diverse range of supergrowing areas and strengths. Supergrowing regions inherently can contain exponentially higher intensities compared to superoscillating regions [11,14]. Therefore, supergrowth will alleviate the effect of enhanced sidelobes plaguing superoscillation-based imaging and improve SNR in experiments. This Letter lays the groundwork for generating supergrowth in the laboratory.

A natural next step is to realize supergrowth-based subwavelength object reconstruction proposed in Ref. [14]. Also, supergrowth being a weak value amplification of momentum [10], generating optical fields with higher supergrowing strengths could be useful in a multitude of applications

as well, including communication and quantum technologies. Furthermore, an optical field spot with simultaneously optimized supergrowing and superoscillating properties could prove to be extremely beneficial for superresolution imaging.

Acknowledgments. We acknowledge insights provided by Abhishek Chakraborty, Arunabh Mukherjee, and Valeria Viteri-Pflucker in this project. This work was supported by the AFOSR Grant No. FA9550-21-1-0322 and the Bill Hannon Foundation.

[1] J. W. Goodman, *Introduction to Fourier Optics*, 4th ed. (W. H. Freeman, Macmillan Learning, New York, 2017).

[2] G. Chen, Z.-Q. Wen, and C.-W. Qiu, Superoscillation: From physics to optical applications, Light: Sci. Appl. **8**, 56 (2019).

[3] G. Gbur, Using superoscillations for superresolved imaging and subwavelength focusing, Nanophotonics **8**, 205 (2019).

[4] M. V. Berry and S. Popescu, Evolution of quantum superoscillations and optical superresolution without evanescent waves, J. Phys. A: Math. Gen. **39**, 6965 (2006).

[5] M. Berry, N. Zheludev, Y. Aharonov, F. Colombo, I. Sabadini, D. C. Struppa, J. Tollaksen, E. T. F. Rogers, F. Qin, M. Hong *et al.*, Roadmap on superoscillations, J. Opt. **21**, 053002 (2019).

[6] K. S. Rogers, K. N. Bourdakos, G. H. Yuan, S. Mahajan, and E. T. F. Rogers, Optimising superoscillatory spots for far-field super-resolution imaging, Opt. Express **26**, 8095 (2018).

[7] Y. Hu, S. Wang, J. Jia, S. Fu, H. Yin, Z. Li, and Z. Chen, Optical superoscillatory waves without side lobes along a symmetric cut, Adv. Photonics **3**, 045002 (2021).

[8] Y. Kozawa, D. Matsunaga, and S. Sato, Superresolution imaging via superoscillation focusing of a radially polarized beam, Optica **5**, 86 (2018).

[9] X. H. Dong, A. M. H. Wong, M. Kim, and G. V. Eleftheriades, Superresolution far-field imaging of complex objects using reduced superoscillating ripples, Optica **4**, 1126 (2017).

[10] A. N. Jordan, Y. Aharonov, D. C. Struppa, F. Colombo, I. Sabadini, T. Shushi, J. Tollaksen, J. C. Howell, and A. N. Vamivakas, Super-phenomena in arbitrary quantum observables, Phys. Rev. A **110**, 012206 (2024).

[11] A. N. Jordan, Superresolution using supergrowth and intensity contrast imaging, Quantum Stud.: Math. Found. **7**, 285 (2020).

[12] D. W. Pohl, W. Denk, and M. Lanz, Optical stethoscopy: Image recording with resolution λ/20, Appl. Phys. Lett. **44**, 651 (1984).

[13] H. Yang, N. Moullan, J. Auwerx, and M. A. M. Gijs, Super-resolution biological microscopy using virtual imaging by a microsphere nanoscope, Small **10**, 1712 (2014).

[14] T. Karmakar, A. Chakraborty, A. N. Vamivakas, and A. N. Jordan, Supergrowth and sub-wavelength object imaging, Opt. Express **31**, 37174 (2023).

[15] T. Karmakar and A. N. Jordan, Beyond superoscillation: General theory of approximation with bandlimited functions, J. Phys. A: Math. Theor. **56**, 495204 (2023).

[16] V. Arrizón, U. Ruiz, R. Carrada, and L. A. González, Pixelated phase computer holograms for the accurate encoding of scalar complex fields, J. Opt. Soc. Am. A **24**, 3500 (2007).

[17] See Supplemental Material at http://link.aps.org/supplemental/10.1103/PhysRevResearch.6.L032043 for further details about the numerical optimization techniques and optical fields used in the experiment.